Korean J. Chem. Eng., 34(4), 1051-1061 (2017)
DOI: 10.1007/s11814-016-0353-6

pISSN: 0256-1115
eISSN: 1975-7220

Magnetic nanocomposite of multi-walled carbon nanotube as effective adsorbent for methyl violet removal from aqueous solutions: Response surface modeling and kinetic study

Mona Ehyaee, Fariba Safa†, and Shahab Shariati

Department of Chemistry, Rasht Branch, Islamic Azad University, Rasht, I. R. Iran
(*Received 2 August 2016 • accepted 17 December 2016*)

Abstract−Magnetic nanocomposite of multi-walled carbon nanotube (m-MWCNT) was synthesized for adsorptive removal of methyl violet (MV) from aqueous solutions. The experiments were conducted using a central composite design (CCD) with the variables of adsorbent dosage (0.4-1.2 g/L), solution pH (3-9), contact time (10-42 min) and ionic strength (0.02-0.1 mol L^{-1}). Regression analysis showed good fit of the experimental data to a quadratic response surface model whose statistical significance was verified by analysis of variance. By applying the desirability functions, optimum conditions of the process were predicted as adsorbent dosage of 0.99 g/L, pH=4.92, contact time of 40.98 minutes and ionic strength of 0.04 mol L^{-1} to achieve MV removal percentage of 101.19. Experimental removal efficiency of 99.51% indicated that CCD along with the desirability functions can be effectively applied for optimizing MV removal by m-MWCNT. Based on the study, the adsorption process followed Langmuir isotherm model and pseudo-second-order kinetic model could realistically describe the dye adsorption onto m-MWCNT.

Keywords: Magnetic Nanocomposite, Multi-Walled Carbon Nanotubes, Response Surface Modeling, Optimization, Methyl Violet Dye, Adsorptive Removal

INTRODUCTION

Contamination of water sources is a serious worldwide environmental problem. According to the World Health Organization (WHO) report, 70-80% of all illnesses in developing countries are related to water contamination, with particular susceptibility for women and children [1]. Advanced technologies of textile, paper, leather tanning, food processing, plastics, cosmetics, drugs and dye manufacturing industries are some of the main sources of water contamination [2-5]. Total dye consumption of the textile industry worldwide is more than 10,000 tons/year and almost 1% of them is discharged into water streams [6]. Since many of the industrial dyes are toxic, carcinogenic, mutagenic and teratogenic [7,8], they play significant role in water pollution. Many researchers throughout the world have focused their efforts on dye removal from effluents by the techniques such as photocatalytic degradation [9], coagulation/flocculation [10], membrane filtration [11], ion exchange [12], adsorption [13-17] and oxidation [18,19].

Among the existing dye removal techniques, adsorption as an uncomplicated, effective and economical technique has received much attention for wastewater treatment. Multi-walled carbon nanotubes (MWCNTs) are known as potent adsorbents for removing various pollutants from different environments due to their unique properties such as small size, hollow and layered structures and large specific surface area [20,21]. In spite of these unique properties, MWCNTs are difficult to separate from aqueous solutions and their residuals may cause secondary pollution [22]. Therefore, separation of the nanoparticles from aqueous solutions is a critical step in water treatment. The nanoparticles are usually separated by centrifuge or filtration, which adds more costs to the adsorption process. Producing magnetic nanocomposite through integration of carbon nanotubes and magnetic particles can overcome the defects of separation inconvenience and pollution problem [23,24]. The magnetic nanocomposites of MWCNT are also of great importance in accelerating separation speed in purifying large amounts of wastewater without producing contaminants [25]. In addition, the nanocomposites make possible their fast online separation from liquid phase by simply applying a magnetic field [26]. In recent years, magnetic nanocomposites of MWCNT and modified MWCNT have been employed as adsorbent for removal of different classes of the synthetic dyes [27-33].

It is well known that adsorption capability of an adsorbent mainly depends on the process variables such as adsorbate concentration, solution pH, adsorbent dosage, contact time, temperature and so on. Therefore, optimizing the variables is essential to achieving maximum efficiency of the dye removal process. Conventional optimization technique, i.e., measuring the response at constant values of the independent variables, suffers the limitations of non-depiction of the combined effect of the independent variables and greater time consumption due to large number of experiments [34,35]. The limitations can be overcome by the empirical statistical technique of response surface modeling (RSM). This technique makes possible to design experiments, build models, evaluate relative significance of the independent variables and their interactions, and to determine optimum conditions for desirable responses. By applying RSM technique, the influence of different variables affecting the

†To whom correspondence should be addressed.
E-mail: Safa@iaurasht.ac.ir

response can be investigated by their simultaneous variation through carrying out a limited number of experiments [36-39]. Some researchers have used RSM to optimize the adsorptive dye removal processes [40-43]. Nevertheless, no information is available in the literature regarding optimization of MV removal by m-MWCNT using response surface modeling. Methyl violet was selected as a target due to its application in dyeing different materials such as cotton, silk, paper, weed and so on. The dye is also used in biomedical fields as active ingredient in Gram staining for bacteria classification [44]. In spite of widespread uses, direct contact with MV can cause pain and congestion, while inhalation can irritate the respiratory and gastrointestinal systems. In addition, MV releases toxic substances such as CO, CO_2 and NO when decomposed [45]. Therefore, concerns exist regarding the ecological impact of the release of methyl violet into the environment.

Our main objectives were: (1) applying a four-factor central composite design for response surface modeling of methyl violet removal from aqueous solutions by m-MWCNT; (2) examination of the effects of four variables of adsorbent dosage, solution pH, contact time and ionic strength and their interactions on the dye removal efficiency; and (3) verification of the response surface model for predicting optimum adsorption conditions of MV onto m-MWCNT. Also, to assess the mechanism of adsorption process and to evaluate the kinetic parameters, we performed a detailed kinetic study.

MATERIALS AND METHODS

1. Chemicals

The chemicals including methyl violet ($C_{24}H_{28}N_3Cl$, N-(4-(bis (4-(dimethylamino) phenyl) methylene) cyclohexa-2,5-dien-1-ylidene) methanaminium chloride), ferrous chloride ($FeCl_2{\cdot}4H_2O$), ferric chloride ($FeCl_3{\cdot}6H_2O$), ammonia (NH_3), sodium hydroxide (NaOH), hydrochloric acid (HCl) and sodium chloride (NaCl) with high purity were purchased from Merck (Darmstadt Germany) and used without further purification. Multi-walled carbon nanotube (98%) with outer diameter of 15-20 nm was purchased from Nanosany corporation (Mashhad, Iran). Accurately weighed quantity of the dye was dissolved in distilled water to prepare 10 mg L^{-1} stock solution. Adjustment of pH was done by the solutions of 0.1 mol L^{-1} NaOH or HCl. Sodium chloride was used for adjusting ionic strength.

2. Analytical Measurements

Absorbance measurements were performed by Milton Roy UV-Vis spectrophotometer (Model 601, U.S.A) using a glass cell (1 cm) at 585 nm as maximum absorption wavelength of Methyl Violet. A Jenway digital pH meter (Model 3305, Germany) with a combined glass electrode was used for pH measurements and a hotplate stirrer (Model IKA RH basic 2, Germany) to stir the dye solutions. Separation of nanocomposite from aqueous solutions was done using a supermagnet ($2\times4\times2.5$ cm^3) with 1.4 T magnetic field.

Size and morphology of the magnetic nanocomposite were characterized by SEM (Model X130, Philips, Netherland). Also, an X-ray diffractometer (XRD, Model 1830, Philips, Netherland) using Cu K_α radiation (λ=0.1541 nm) was used for determination of the crystal structure of the magnetic nanocomposite at ambient temperature. Identification of functional groups of the nanocomposite was performed using a FTIR spectrometer (Model AIM 880, Shimadzu, Japan) in the spectral range of 4,000-400 cm^{-1}.

3. Synthesis of the Nanocomposite

Magnetic components were introduced into multi-walled carbon nanotubes by using chemical coprecipitation [46]. At first, 100 mL of an aqueous solution in the mole ratio of Fe^{2+} : Fe^{3+}=1 : 2 was prepared by addition of some drops of concentrated HCl for complete dissolution of the iron salts. Then, commercial MWCNT was suspended in the solution with the mass ratio of 1 : 5 (MWCNT : Fe^{2+}+Fe^{3+}). Finally, 500 mL of 1.5 mol L^{-1} NH_3 was added dropwise till pH reached 11-12. Whole reaction was performed in the temperature range of 80-90 °C with constant stirring rate under nitrogen atmosphere till the suspension changed to black color. Then, the mixture was stirred for further 30 minutes to complete the reaction. After cooling to room temperature, the product was isolated from the mixture by the supermagnet, washed with double distilled water for several times, and dried at 100 °C for 2 hours.

4. Batch Adsorption Experiments

Adsorption studies of methyl violet onto m-MWCNT were performed by the batch experiments. In each experimental run, the aliquots of MV sample (50 mL, 10 mg L^{-1}) with known pH, ionic strength and adsorbent dosage were agitated by stirring at constant speed at room temperature. Then, at appropriate time, the magnetic nanoadsorbent was isolated from the suspension and the supernant was analyzed for the dye residual. The dye removal efficiency (Y%) by m-MWCNT was calculated using the following equation:

$$Y\ (\%)=\left[\frac{C_0-C_t}{C_0}\right]\times 100 \quad (1)$$

where C_0 and C_t are the initial and final dye concentrations in the solution (mg L^{-1}), respectively.

5. Central Composite Experimental Design

Central composite design is one of the most popular RSM designs for modeling the relationship between the experimental factors and the observed responses. The design makes possible to optimize chemical processes through three major steps: (i) performing statistically designed experiments, (ii) developing a significant mathematical model, and (iii) predicting the optimum responses throughout the experimental space [38]. We used CCD to study the effects of four input variables, including adsorbent dosage, solution pH, contact time, and ionic strength, on methyl violet removal efficiency by m-MWCNT and to find the optimum conditions of the process. Constant concentration of MV (10 mg L^{-1}) was used as a fixed input parameter. Experimental range of the process variables and coded design matrix are given in Tables 1 and 2, respectively. As shown, CCD consisted of a two-level full-factorial design (runs of 1-16); star points at a distance α from design center (runs of 17-24); and the center point (runs of 25-30) to provide information about existence of curvature in the system. The distance α was computed as $\alpha=(2n)^{1/4}$ where n equals the number of the process variables [47]. To ensure that no uncontrolled variable affected the results in a systematic way, the experiments were conducted in a random order. A nonlinear regression method was used to fit the quadratic polynomial to the experimental data. Considering all linear, second-order and interaction terms, a quadratic response model for two input variables of X_i and X_j can be described as:

Table 1. Experimental variables and corresponding level settings

Variable	Symbol	$-\alpha$	−1	0	+1	$+\alpha$
Adsorbent dose (g L^{-1})	A	0.4	0.6	0.8	1.0	1.2
pH	B	3.0	4.5	6.0	7.5	9.0
Time (min)	C	10	18	26	34	42
Ionic strength (mol L^{-1})	D	0.02	0.04	0.06	0.08	0.10

Table 2. CCD matrix in coded values and experimental removal efficiencies of MV by m-MWCNT nanocomposite

Experiment	Run	A (g/L)	B	C (min)	D (mol L^{-1})	Y (%)
1	23	−1	−1	−1	−1	68.00
2	4	+1	−1	−1	−1	91.00
3	21	−1	+1	−1	−1	77.20
4	28	+1	+1	−1	−1	97.10
5	12	−1	−1	+1	−1	53.90
6	3	+1	−1	+1	−1	95.00
7	18	−1	+1	+1	−1	57.50
8	11	+1	+1	+1	−1	99.00
9	22	−1	−1	−1	+1	79.50
10	6	+1	−1	−1	+1	85.50
11	24	−1	+1	−1	+1	91.20
12	2	+1	+1	−1	+1	79.10
13	13	−1	−1	+1	+1	73.70
14	7	+1	−1	+1	+1	96.40
15	17	−1	+1	+1	+1	80.90
16	8	+1	+1	+1	+1	98.40
17	1	$-\alpha$	0	0	0	55.40
18	5	$+\alpha$	0	0	0	98.60
19	16	0	$-\alpha$	0	0	97.30
20	25	0	$+\alpha$	0	0	93.50
21	14	0	0	$-\alpha$	0	89.65
22	20	0	0	$+\alpha$	0	90.00
23	15	0	0	0	$-\alpha$	60.80
24	26	0	0	0	$+\alpha$	70.70
25	29	0	0	0	0	86.00
26	9	0	0	0	0	83.75
27	19	0	0	0	0	84.15
28	30	0	0	0	0	86.00
29	10	0	0	0	0	88.00
30	27	0	0	0	0	88.00

$$Y=\beta_0+\Sigma\,\beta_i X_i+\Sigma\,\beta_{ii}X_{ii}^2+\Sigma\,\beta_{ij}X_{ij}+\varepsilon \quad (2)$$

where Y is the predicted response (dye removal efficiency) and ε is the residual error. Also, β_0 is the model constant and the coefficients of β_i, β_{ii} and β_{ij} are the linear, quadratic and interaction effects of the input variables, respectively.

RESULTS AND DISCUSSION

1. Characterization of the Magnetic Nanocomposite

Particle size and morphology of the synthesized m-MWCNT nanocomposite were examined by SEM imaging. The SEM image in Fig. 1 clearly indicates that the surface of MWCNTs has been

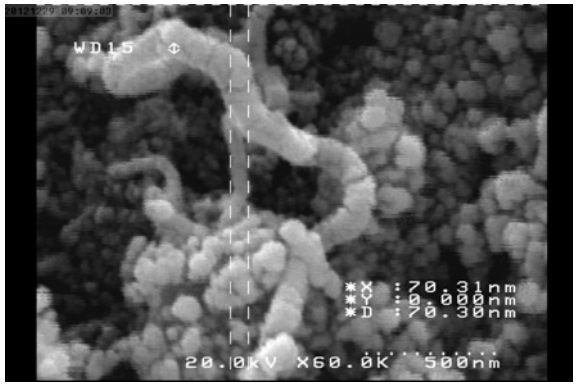

Fig. 1. SEM image of the synthesized magnetic nanocomposite of MWCNT.

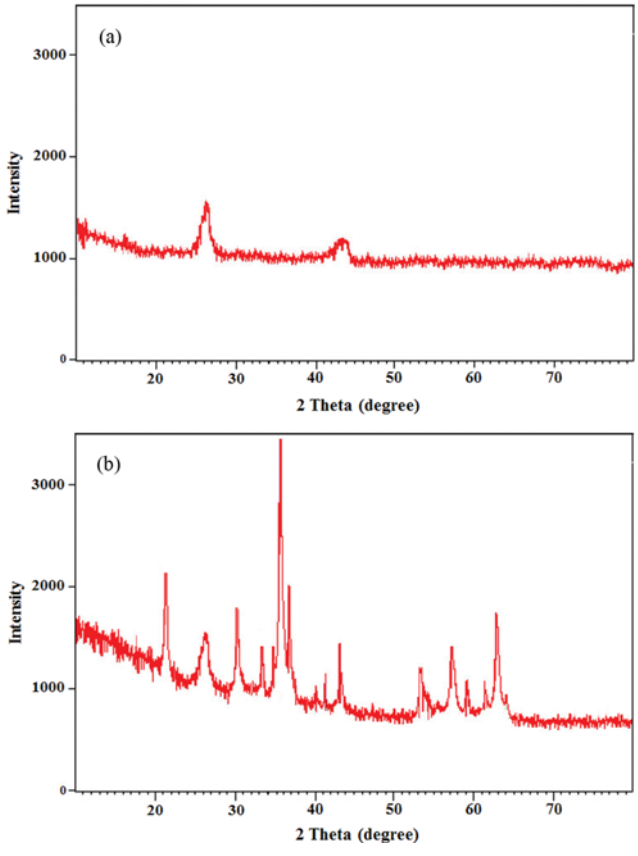

Fig. 2. XRD pattern of bare MWCNT (a) and m-MWCNT nanocomposite (b).

successfully coated by Fe_3O_4 nanoparticles with approximate size of 50 nm. Fig. 2 shows XRD patterns of the bare MWCNT and the magnetic nanocomposite.

As shown, the characteristic peaks of MWCNT at 2θ=26.2° and 43.3° (Fig. 2(a)) also exist in the XRD pattern of the nanocomposite (Fig. 2(b)). The XRD pattern in Fig. 2(b) also displays six characteristic peaks of iron oxide nanoparticles. They include four peaks at 2θ=30.3°, 35.6°, 43.3°, 57.3° related to maghemite or magnetite [48] and two peaks at 2θ=53.7° and 62.8° that may be assigned to hematite [49]. The diffraction peaks can be well indexed to the (2 2 0), (3 1 1), (4 0 0), (5 1 1), (4 2 2), and (4 4 0) planes, respectively (JCPDS No.19-0629), indicating that resultant magnetic nanoparticles were Fe_3O_4 with a typical inversed spinel cubic structure. The other peaks at 2θ=26.2° and 43.3° correspond to the structure of MWCNTs.

Surface chemistry of the nanocomposite was studied using FTIR spectrum. Fig. 3 indicates the FTIR spectrum for the magnetic nanocomposite. The broad peak at about 3,450 cm^{-1} refers to the stretching vibrations of hydroxyl groups due to partial oxidation of the surface of MWCNTs. Moreover, the peak at ~1,650 cm^{-1} may be assigned to the stretching vibrations of the carbon nanotube backbone [50]. Based on the previous reports, Fe-O bond of bulk Fe_3O_4 shows two characteristic absorption bands at 375 and 570 cm^{-1} [51]. In Fig. 3, these bands have shifted to about 440 and 600 cm^{-1}, respectively and the later band has splitted into the peaks at 631.4 and 582.9 cm^{-1}. The changes in peak positions may result from the fact that the surface bond force constant increases as Fe_3O_4 is reduced to nanodimension, so that the absorption bands of IR spectrum shift to higher wavenumbers [52]. In addition, the band splitting is due to splitting of the energy levels of the quantized Fe_3O_4 nanoparticles [53].

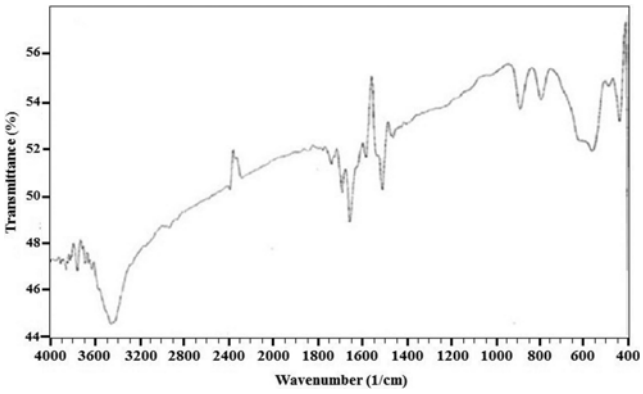

Fig. 3. FTIR spectrum of the magnetic nanocomposite of MWCNT.

2. Response Surface Modeling of the Dye Removal Efficiency

As mentioned, response surface modeling method was followed to investigate both individual and interactive effects of the process variables on the dye adsorption efficiency of the synthesized mag-

Table 3. The statistical parameters of the models developed for MV removal by m-MWCNT nanocomposite

Model	Standard deviation	F	P value	PRESS	R^2	Adjusted R^2	Predicted R^2
Linear	9.81	7.13	0.0006	3729.84	0.5329	0.4581	0.2762
2-Factor interaction	8.16	2.86	0.0371	2285.83	0.7545	0.6253	0.5564
Quadratic	3.12	28.71	<0.0001	770.69	0.9716	0.9452	0.8504
Cubic	1.88	4.29	0.0352	1215.73	0.9952	0.9801	0.7641

Table 4. Results of ANOVA for the quadratic model

Source	Sum of squares	df	Mean square	F	P value	Remark
Model	5007.10	14	357.65	36.70	<0.0001	
A	2521.50	1	2521.50	258.77	<0.0001	Highly significant
B	37.00	1	37.00	3.80	0.0703	Significant
C	7.15	1	7.15	0.73	0.4051	-
D	180.40	1	180.40	18.51	0.0006	Highly significant
AB	42.25	1	42.25	4.34	0.0549	Significant
AC	462.25	1	462.25	47.44	<0.0001	Highly significant
AD	522.12	1	522.12	53.58	<0.0001	Highly significant
BC	0.90	1	0.90	0.093	0.7651	-
BD	4.41	1	4.41	0.45	0.5113	-
CD	110.25	1	110.25	11.31	0.0043	Highly significant
A^2	123.98	1	123.98	12.72	0.0028	Highly significant
B^2	167.88	1	167.88	17.23	0.0009	Highly significant
C^2	32.01	1	32.01	3.28	0.0900	Significant
D^2	668.96	1	668.96	68.65	<0.0001	Highly significant
Residual	146.16	15	9.74	-	-	-
Lack of fit	129.68	10	12.97	3.93	0.0719	Nonsignificant
Pure error	16.48	5	3.30	-	-	-

netic nanocomposite. Values of the response variable (Y%) measured according to CCD matrix are listed in Table 2. Polynomial regression modeling was performed between the response variable and the four process variables with assuming that the higher order interaction effects are negligible relative to the two-way interactions. Table 3 presents statistical characteristics of the linear, interactive, quadratic and cubic models fitted to the experimental data. Based on the results, a quadratic model was found to be the best response surface model for the adsorption process. The developed model in terms of the coded input variables is as follows:

$$Y=85.98+10.25\,A+1.24\,B-0.55\,C+2.74\,D-1.62\,AB+5.38\,AC-5.71\,AD-0.24\,BC-0.52\,BD+2.63\,CD-2.13\,A^2+2.47\,B^2+1.08\,C^2-4.94\,D^2 \quad (3)$$

As is evident from the correlation coefficient value (R^2), the model explains more than 97% of variation in the experimental data. Also, the adjusted correlation coefficient (R^2_{adj}), that corrects R^2 value for sample size and number of model terms, was found to be very close to R^2 showing high significance of the quadratic model. Moreover, considerably high predicted R^2 and low value of predicted residual sum of square (PRESS) suggest for reasonable predictive ability of the model.

Adequacy and statistical significance of the quadratic model were also evaluated by analysis of variance (ANOVA) [43]. Table 4 lists the results of ANOVA for the quadratic model. Fisher ratio value of 36.7 shows a high degree of statistical credibility and an excellent fit of the model to the response values. Moreover, $p<0.0001$ implies the model is significant at 99.99% confidence level. The results also indicate that the lack of fit is not significant relative to the pure error. Based on ANOVA results, the main effects of A and D, interaction effects of AC, AD and CD and second-order effects of A^2, B^2 and D^2 are highly significant to the response at 99% of confidence level. The terms of B, AB and C^2 have also significant effects on the response at 90% of confidence level. Fig. 4 indicates high correlation between the measured and predicted response values for adsorption of MV on m-MWCNT nanocomposite, showing goodness of fit of the developed model. We did further adequacy checking of the model by analyzing the normality of the residuals. Normal probability plot of the residuals in Fig. 5 indicates that the proposed model is adequate because the residuals for the responses are less than 5.5% and tend to be close to the diagonal line.

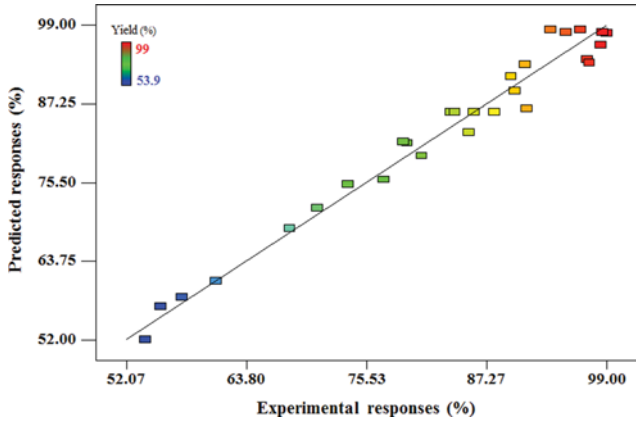

Fig. 4. Scatter plot of the predicted versus experimental responses for MV-nanoadsorbent system.

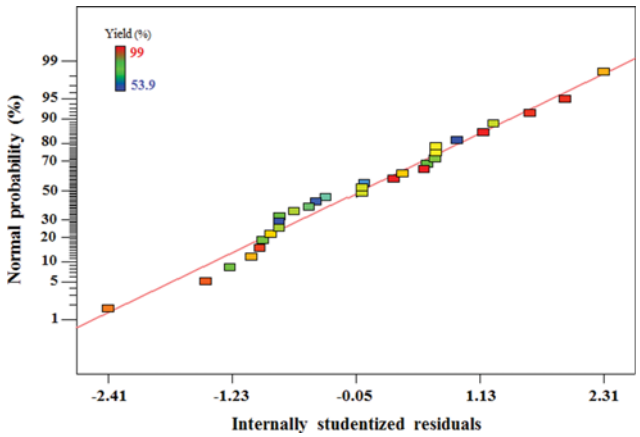

Fig. 5. Normal probability plot of the residual errors.

To determine the contribution of model parameters in the process efficiency, the percent contribution (PC) values were calculated using the following equation [54]:

$$PC=\frac{SS}{\Sigma SS}\times 100 \quad (4)$$

where SS is sum of squares for the individual term and the nominator is sum of SS values for all the model parameters. In Fig. 6, PC values for the components of the developed model are compared. As shown, the highest level of contribution (PC >51.65%) belonged to the adsorbent dosage. Contributions of the two-factor interaction terms of AC, AD and BD in the dye removal efficiency by m-MWCNT nanocomposite were greater than 9% and BC term had minimum contribution.

For accurate understanding of the significant two-factor interaction effects on the dye removal efficiency by m-MWCNT, response surface 3D plots as a function of the two independent variables,

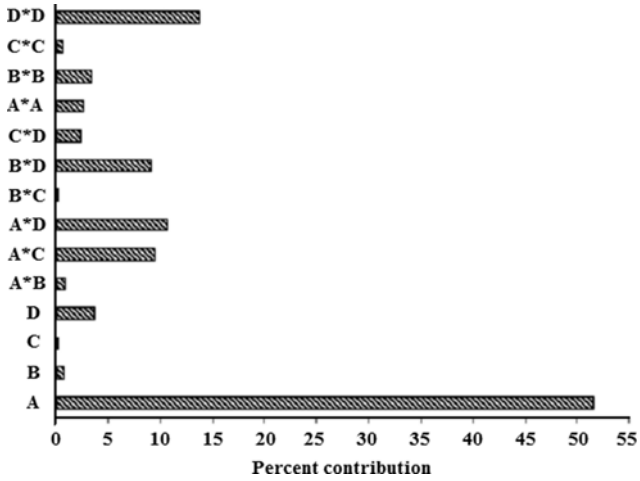

Fig. 6. Comparison of the percent contributions for the components of the quadratic response surface model.

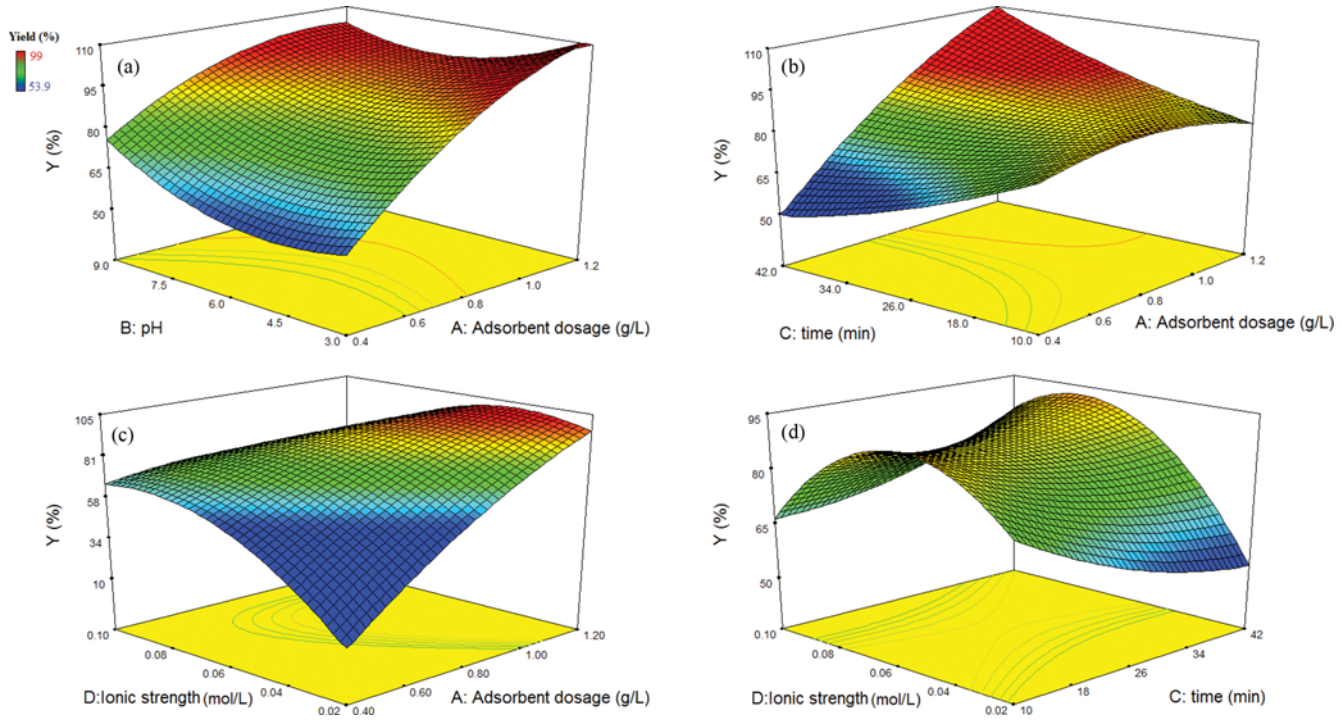

Fig. 7. 3D response surface plots for the two-factor interaction effects of adsorbent dose and pH (a), adsorbent dose and contact time (b), adsorbent dose and ionic strength (c) and ionic strength and contact time (d) for MV-nanoadsorbent system.

maintaining other variables at their middle levels were used. Fig. 7(a) shows the significant combined effect of adsorbent dosage and pH on the adsorption efficiency of MV by m-MWCNT nanocomposite at contact time of 26 minutes and ionic strength of 0.06 mol L^{-1}. As can be easily found, the process efficiency increases with increasing adsorbent dosage due to greater surface area and availability of more adsorption sites for the dye. Also, the figure indicates that pH effect on the response depends on the adsorbent dosage. The dye removal efficiency increases with increasing pH at low to medium levels of the adsorbent. According to the available data, the point of zero charge for m-MWCNT is about 3 [27], and hence, the charge sign on the surface of the adsorbent is negative at pH>3, which favors uptake of MV because of the electrostatic attraction between the adsorbent surface and the cationic dye. Nevertheless, the pH effect on the response is not considerable at high adsorbent dosage, and dye removal efficiency reaches to greater than 95% in all pH values. This observation may be attributed to very high level of contribution of adsorbent dosage (PC= 51.65%) in the process efficiency as compared to pH (PC=0.75%) that covers the pH effect.

Fig. 7(b) indicates the highly significant interactive effect of the adsorbent dosage and contact time on the process efficiency at constant ionic strength of 0.06 mol L^{-1} and pH=6. As expected, the dye uptake is greater than 95% with simultaneous increase in both variables. Also, the plot indicates that above an adsorbent dosage of 0.8 g L^{-1} the process efficiency increases with increasing contact time. Nevertheless, contact time has inverse effect on the response below 0.8 g L^{-1} adsorbent, which may be due to fast saturation of the adsorbent by MV and subsequent desorption of the molecules when stirring continues for more time.

The two-factor interaction effect of the adsorbent dosage and ionic strength on MV adsorption onto m-MWCNT at pH=6 and contact time of 26 minutes is demonstrated in Fig. 7(c). As shown, although the dye uptake by the adsorbent increases with increasing adsorbent dosage, it decreases with increasing ionic strength. This behavior can be explained by the fact that an increase in ionic strength will decrease the adsorption capacity when attractive electrostatic forces exist between the adsorbent surface and adsorbate [55]. The experimental data of the study follow this convention, suggesting that the presence of salt ions in the solution, decreases accessible negative charged adsorption sites of the adsorbent for the cationic dye molecules through occupation of the adsorption sites.

A 3D plot for combined effect of ionic strength and contact time on the dye removal efficiency at constant adsorbent dosage of 0.8 g L^{-1} and pH=6 is given in Fig. 7(d). As it is evident, MV removal percentage does not exceed 92% that corresponds to the data from other plots where achieving removal percentage of greater than 95% needs more than 0.8 g L^{-1} adsorbent. The saddle-like plot shows that at each time, increasing ionic strength causes an increase in the response to the maximum and further increase in the ionic strength decreases the response. Initial increase in the response may be due to decreasing dye solubility in presence of salt that favors dye adsorption onto the nanocomposite. On the other hand, the addition of more salt to the solution can decrease adsorption sites of m-MWCNT that decreases dye adsorption efficiency. Moreover, the plot demonstrates that increasing contact time does not considerably change the response at different levels of ionic strength, probably due to the very small contribution of contact time (PC=0.14%) to the process efficiency as compared to

ionic strength (PC=3.69%).

3. Optimization Using the Desirability Functions

To find the optimum settings of the input variables for achieving maximum efficiency of the process, we used the desirability function approach proposed by Derringer and Suich [56], included in the Design Expert software [57]. In the first step of the approach, each variable (i) was converted into an individual scale-free desirability function (d_i) ranged from 0 (outside of the desired limits) to 1 (at the target value). The desired goals were chosen as within range (for the input variables) and maximize (for the response variable), respectively, and the weight of 3 was assigned to the response due to its importance. Then, the goals for all n variables were combined into an overall desirability function (D) whose maximum gives the best global compromise in the studied domain and corresponds to the optimal experimental conditions:

$$D=(d_1\times d_2\times\ldots\times d_n)^{1/n} \quad (5)$$

The goal seeking was begun at random starting points and proceeded up the steepest slope to a maximum. By seeking in the response surfaces, the best local maximum was found to be at adsorbent dosage of 0.99 g/L, pH=4.92, contact time of 40.98 minutes and ionic strength of 0.04 mol L^{-1} for obtaining MV removal percentage of 101.19. Fig. 8 shows the desirability ramp, generated from 25 optimum points via numerical optimization. To support the data given by numerical modeling, confirmatory experiments were conducted using the optimized parameters. The experiments resulted in the removal efficiency of 99.51% with a deviation of 1.6% from the predicted value, pointing out the good accuracy of the model.

4. Adsorption Kinetic Studies

Modeling of the adsorption kinetics allows one to develop suitable sorption rate expressions and to characterize possible reaction mechanisms. To investigate kinetics of the adsorption process of MV onto m-MWCNT, three kinetic models including pseudo-first-order, pseudo-second-order and intraparticle diffusion models were used.

The pseudo-first-order kinetic model can be described as the following equation:

Table 5. Kinetic parameters for MV removal by magnetic MWCNT nanocomposite

Kinetic model	Parameters
Pseudo first-order	
R^2	0.6335
k_1 (min^{-1})	0.00014
q_e (mg g^{-1})	9.373
Pseudo second-order	
R^2	0.9999
k_2 (g $mg^{-1}min^{-1}$)	0.666
q_e (mg g^{-1})	10.395
h (mg g^{-1} min)	76.92
Intraparticle diffusion	
$k_{id,1}$ (mg g^{-1} $min^{-1/2}$)	0.3194
$k_{id,2}$ (mg g^{-1} $min^{-1/2}$)	0.0375
C (mg g^{-1})	9.2904

$$\mathrm{Log}(q_e-q_t)=\log q_e-\frac{k_1}{2.303}t \quad (6)$$

where q_e (mg g^{-1}) is the adsorption capacity at equilibrium, q_t (mg g^{-1}) is amount of the adsorbate at any time t (min) and k_1 (min^{-1}) is the pseudo-first-order rate constant [58].

The pseudo-second-order kinetic model assumes the rate limiting step is surface adsorption of chemisorption nature and can be represented as follows [59]:

$$\frac{t}{q_t}=\frac{1}{k_2q_e^2}+\frac{1}{q_e}t \quad (7)$$

where k_2 (g $mg^{-1}min^{-1}$) is the pseudo-second-order rate constant. Using the equation, the initial sorption rate, h (mg g^{-1} min) can be calculated as:

$$h=k_2q_e^2 \quad (8)$$

Table 5 presents the kinetic parameters calculated using different kinetic equations. As shown, the obtained correlation coefficients for the plots of log (q_e-q_t) versus t and t/q_t versus t (not shown)

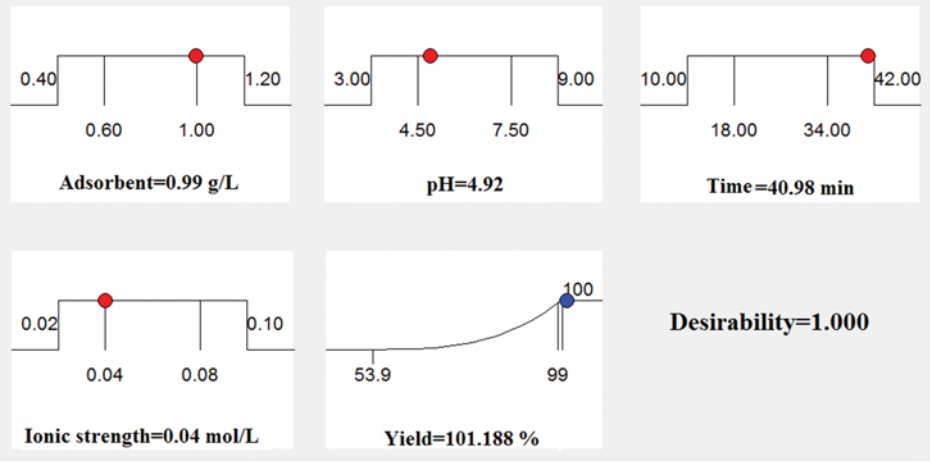

Fig. 8. Desirability ramp for the numerical optimization of the selected goals.

were 0.6335 and 0.9999, respectively. Hence, it can be found that the pseudo second-order model can approximate more accurately the adsorption kinetics suggesting chemisorption of MV onto m-MWCNT. Moreover, the initial sorption rate for MV adsorption onto the nanocomposite is 76.92 mg g^{-1} min, showing relatively fast dye adsorption at beginning of the process.

Intraparticle diffusion or Morris-Weber model is an empirically found functional relationship that is common to most adsorption processes. The model is applicable for the processes where the adsorption rate depends on the speed at which adsorbate diffuses towards the adsorbent. Based on the model, the diffusion-controlled adsorption processes follow a linear relationship between the adsorbate uptake (q_t in mg g^{-1}) and square root of time [60].

$$q_t = k_{id} t^{1/2} + C \quad (9)$$

where k_{id} is intraparticle diffusion rate constant (g $mg^{-1}min^{-1}$) and the intercept C is a constant whose value is proportional to the thickness of the boundary layer [61]. Fig. 9 shows fitting of the experimental data to the intraparticle diffusion model for MV-nanocomposite system. The figure consists of two distinct linear regions related to the phases of macropore and micropore diffusions, respectively [62]. The first sharper region is attributed to the external mass transfer involving diffusion of MV molecules into the most readily available adsorbing sites on the adsorbent surface. In this phase, about 98% of MV was uptaken by m-MWCNT within at $t^{1/2}$ value of about 3 min and manifests an average rate of uptake of about 3.41 mg $g^{-1}min^{1/2}$. The second phase is gradual adsorption stage where intraparticle diffusion is rate limiting. This phase involves slow diffusion of the adsorbate from the surface into the micropores of the adsorbent, which in turn stimulates a very slow migration of the adsorbate from the liquid phase onto the adsorbent surface. Table 5 lists the values of k_{id} for the two adsorption phases as obtained from the slopes of the straight lines in Fig. 9. Deviation of the intercept from origin shows that the intraparticle diffusion is not the only rate-limiting step and boundary layer control may be involved in the process [63].

5. Adsorption Isotherm Studies

To determine the maximum adsorption capacity of m-MWCNT nanocomposite and to provide more information about the adsorption mechanism, experimental data were analyzed using well-known Langmuir, Freundlich and Tempkin isotherms.

The Langmuir theory presumes a specific homogeneous adsorption onto the adsorbent and can be expressed using the following linear equation [64]:

$$\frac{1}{q_e} = \frac{1}{q_m} + \frac{1}{q_m K_L C_e} \quad (10)$$

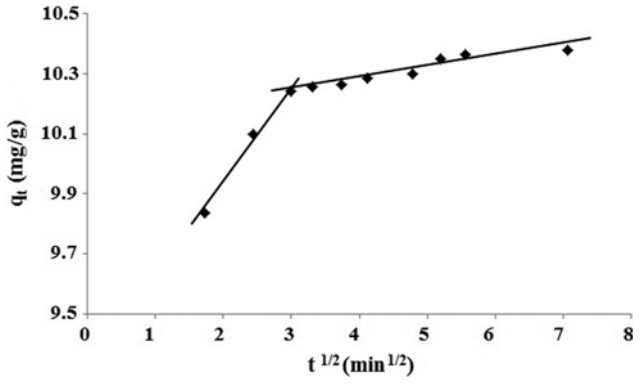

Fig. 9. Intraparticle diffusion plot for MV adsorption onto m-MWCNT (dye concentration=10 ppm, adsorbent dosage=0.99 g/L, pH=4.92 and ionic strength of 0.04 mol L^{-1}).

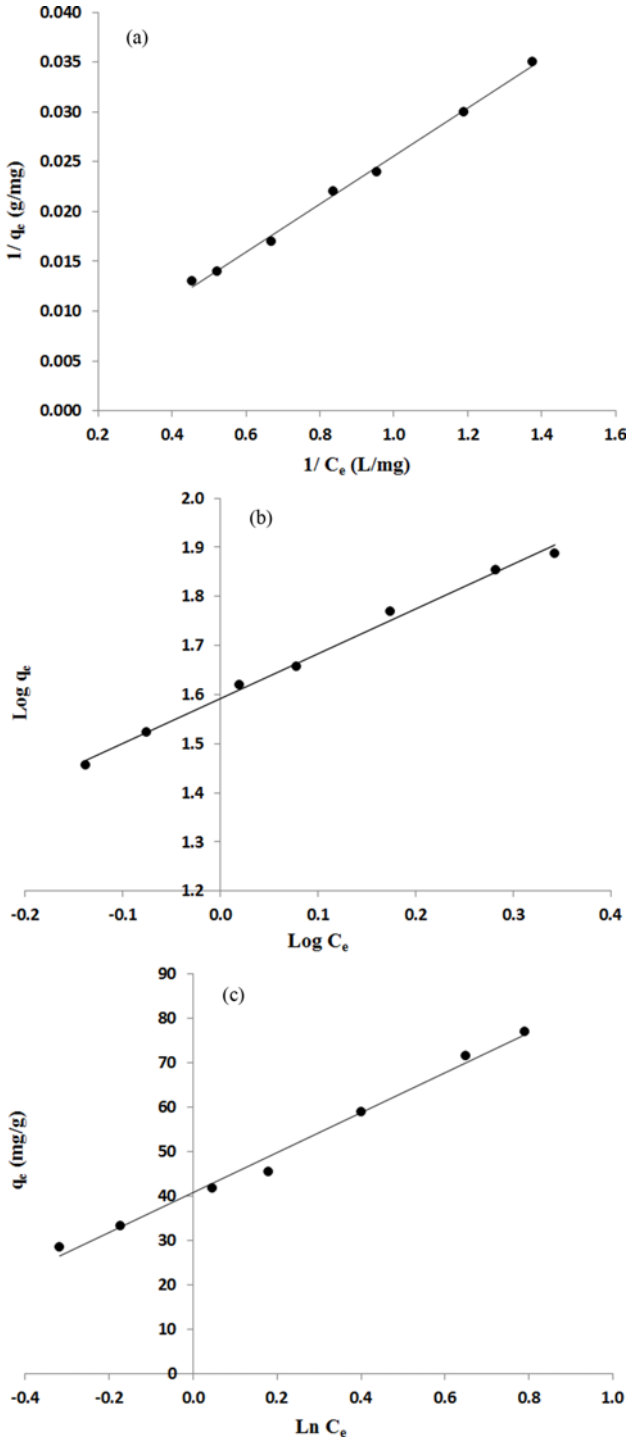

Fig. 10. Langmuir (a), Freundlich (b) and Tempkin isotherms for MV adsorption onto the m-MWCNT nanocomposite.

where q_e and q_m (both in mg g^{-1}) are the equilibrium amount of the adsorbed dye and maximum adsorption capacity of the adsorbent corresponding to monolayer coverage, respectively. The parameter C_e (mg L^{-1}) is equilibrium concentration of the adsorbate and K_L is Langmuir constant (L mg^{-1}).

The Freundlich isotherm assumes that adsorption process occurs onto the heterogeneous surfaces and the adsorption capacity is related to the equilibrium concentration of the adsorbate. Linear form of the Freundlich model is as follows [65]:

$$\text{Log } q_e = \text{Log } K_F + \frac{1}{n} \text{Log } C_e \quad (11)$$

where n is adsorption intensity and the Freundlich constant, K_F ($(mg \cdot g^{-1})(L \cdot mg^{-1})^{1/n}$), is roughly an indicator of the adsorption capacity.

According on the Tempkin isotherm, the adsorption process is characterized by a uniform distribution of binding energies, and the heat of the process decreases linearly with adsorbent coverage due to adsorbent-adsorbate interactions. Tempkin isotherm is represented as follows [66]:

$$q_e = \beta \text{Ln } k_t + \beta \text{Ln } C_e \quad (12)$$

where β is a constant related to the heat of adsorption and k_t is the equilibrium binding constant (L g^{-1}) related to maximum binding energy.

The linearized Langmuir, Freundlich and Tempkin isotherms are shown in Fig. 10 and corresponding parameters are given in Table 6. Based on the obtained correlation coefficients (R^2), the Langmuir isotherm was found to be the best model to fit the experimental adsorption data, indicating that the adsorption process occurred almost on homogeneous surfaces. The maximum adsorption capacity using the model was found to be 666.7 mg g^{-1}, which indicates that the nanocomposite provided a large number of adsorbing sites for MV adsorption.

To determine the favorability of the adsorption process, the Langmuir constant was used to calculate the dimensionless separation factor of R_L by the following equation [65]:

$$R_L = \frac{1}{1 + K_L C_o} \quad (13)$$

where C_o is the initial dye concentration (mg L^{-1}). The adsorption process is irreversible when R_L equals 0, favorable when it is between 0 and 1.0, linear when R_L equals 1.0, and unfavorable when it is greater than 1.0. The obtained value of 0.616 for R_L in the study showed that MV adsorption onto m-MWCNT was favorable.

According to the data in Table 6, the experimental data also correspond to the Freundlich model with R^2 value lower than the one obtained for Langmuir model. The value of less than 1 for 1/n confirms that m-MWCNT is a suitable adsorbent for MV removal from aqueous solutions. Tempkin isotherm model resulted in the value of 40.776 for β and 3.014 L g^{-1} for the equilibrium binding constant. A comparison of the maximum adsorption capacity of m-MWCNT nanocomposite and some other nanoadsorbents for MV removal from aqueous solutions is given in Table 7. It is clear that the nanocomposite used in the present work resulted in very satisfactory efficiencies when compared to the other nanoadsorbents.

Table 6. Isotherm parameters for adsorption of MV onto the magnetic MWCNT nanocomposite

Isotherm model	Parameters
Langmuir	
R^2	0.9968
q_m (mg g^{-1})	666.7
K_L (L mg^{-1})	0.062
Freundlich	
R^2	0.9940
K_F ($(mg \cdot g^{-1})(L \cdot mg^{-1})^{1/n}$)	39.093
1/n	0.909
Tempkin	
R^2	0.9904
K_t (L g^{-1})	3.014
β	40.776

CONCLUSION

We studied adsorptive removal of Methyl Violet from aqueous solutions by m-MWCNT nanocomposite. The main and interactive effects of the experimental parameters, including adsorbent dosage, pH, contact time and ionic strength, were studied using the response surface method based on a central composite design. We found that a quadratic regression model could properly interpret the experimental data. Among the main effects, the highest level of contribution to the response (>50%) belonged to the adsorbent dosage. Moreover, the two-factor interaction term of adsorbent dosage and ionic strength showed higher contribution to MV removal efficiency than the other interaction terms. Simultaneous optimization of the parameters by the desirability functions resulted in an experimental efficiency of 99.51% for MV adsorption onto m-MWCNT. Small deviation of the result from the predicted response verified reliability and effectiveness of the combination of the response surface method and desirability functions for optimizing Methyl Violet removal from aqueous solutions using mag-

Table 7. Comparison of maximum adsorption capacity of different nanoadsorbents for MV removal

Adsorbent	q_m (mg g^{-1})	Reference
SDS modified Fe_3O_4 nanoparticles	416.7	[68]
Hydrolyzed polyacrylamide grafted xanthan gum/SiO_2 nanocomposite	378.8	[69]
Gum xanthan/Fe_3O_4 based nanocomposite hydrogel	642.0	[70]
m-MWCNT nanocomposite	666.7	This work

netic nanocomposite of MWCNT. Adsorption kinetic of Methyl Violet onto m-MWCNT followed the pseudo second-order rate expression with initial sorption rate of 76.92 mg g^{-1}.

REFERENCES

1. WHO/UNICEF, *Global Water Supply and Sanitation Assessment Report 2000*, WHO, Geneva (2000).
2. M. Rafatullah, O. Sulaiman, R. Hashim and A. Ahmad, *J. Hazard. Mater.*, **177**, 70 (2010).
3. B. Amith, D. Sivanesan, K. Kannan and C. Tapan, *Appl. Microbiol. Biotechnol.*, **74**, 1145 (2007).
4. A. K. Samanta and P. Agarwal, *J. Fiber Text. Res.*, **34**, 384 (2009).
5. P. Monash and G. Pugazhenthi, *Adsorption*, **15**, 390 (2009).
6. M. T. Yagub, T. K. Sen and H. Ang, *Water Air Soil Pollut.*, **223**, 5267 (2012).
7. H. A. Mekkawy, M. O. Ali and A. M. El-Zawahry, *Toxicol. Lett.*, **95**, 155 (1998).
8. D. A. Oxspring, G. McMullan, W. F. Smyth and R. Marchant, *Biotechnol. Lett.*, **18**, 527 (1996).
9. Q. Zhang, G. Meng, J. Wu, D. Li and Z. Liu, *Opt. Mater.*, **46**, 52 (2015).
10. S. S. Moghaddam, M. R. A. Moghaddam and M. Arami, *J. Hazard. Mater.*, **175,** 651 (2010).
11. C.-H. Lin, C.-H. Gung, J. J. Sun and S.-Y. Suen, *J. Membr. Sci.*, **471**, 285 (2014).
12. M. Wawrzkiewicz, *Chem. Eng. J.*, **217**, 414 (2013).
13. A. Ozcan and A. S. Ozcan, *J. Hazard. Mater.*, **125**, 252 (2005).
14. L. Zhong, C. Lee and F. Haghighat, *J. Hazard. Mater.*, **243**, 340 (2012).
15. O. Duman, S. Tunc and T. G. Polat, *Micropor. Mesopor. Mater.*, **210**, 176 (2015).
16. E. Ayranci and O. Duman, *Sep. Sci. Technol.*, **44**, 3735 (2009).
17. O. Duman, S. Tunç and T. G. Polat, *Appl. Clay Sci.*, **109-110**, 22 (2015).
18. S. Tunç, O. Duman and T. Gürkan, *Ind. Eng. Chem. Res.*, **52**, 1414 (2013).
19. S. Tunç, T. Gürkan and O. Duman, *Chem. Eng. J.*, **181-182**, 431 (2012).
20. W. W. Tang, G. M. Zeng, J. L. Gong, Y. Liu, X. Y. Wang, Y. Y. Liu, Z. F. Liu, L. Chen, X. R. Zhang and D. Z. Tu, *Chem. Eng. J.*, **211**, 470 (2012).
21. L. Maggini, J.-M. Raquez, R. Marega, J. Jensen Ahrens, F. Pineux, F. Meyer, P. Dubois and D. Bonifazi, *Chem. Sus. Chem.*, **6**, 367 (2013).
22. L. Ai, H. Huang, Z. Chen, X. Wei and J. Jiang, *Chem. Eng. J.*, **156**, 243 (2010).
23. W. Konicki, I. Pelech, E. Mijowska and I. Jasinska, *Chem. Eng. J.*, **210**, 87 (2012).
24. Y. Liu, W. Jiang, Y. Wang, X. J. Zhang, D. Song and F. S. Li, *J. Magn. Magn. Mater.*, **321**, 408 (2009).
25. R. Sivashankar, A. B. Sathya, K. Vasantharaj and V. Sivasubramanian, *Environ. Nanotechnol. Monit. Manage.*, **1-2**, 36 (2014).
26. S. S. Banerjee and D. H. Chen, *J. Hazard. Mater.*, **147**, 792 (2007).
27. J.-L. Gong, B. Wang, G.-M. Zeng, Ch.-P. Yang, Ch.-G. Niu, Q.-Y. Niu, W.-J. Zhou, and Y. Liang, *J. Hazard. Mater.*, **164**, 1517 (2009).
28. T. Madrakian, A. Afkhami, M. Ahmadi and H. Bagheri, *J. Hazard. Mater.*, **196**, 109 (2011).
29. T. Madrakian, A. Afkhami, N. Rezvani Jalal and M. Ahmadi, *Sep. Sci. Technol.*, **48**, 2638 (2013).
30. N. Dalali, M. Habibizadeh, K. Rostamizadeh and S. Nakisa, *Asia Pac. J. Chem. Eng.*, **9**, 552 (2014).
31. Ş. S. Bayazit, *Sep. Sci. Technol.*, **49**, 1389 (2014).
32. O. Duman, S. Tunç, T. G. Polat and B. K. Bozoğlan, *Carbohydr. Polym.*, **147**, 79 (2016).
33. O. Duman, S. Tunç, B. K. Bozoğlan and T. G. Polat, *J. Alloy. Compd.*, **687**, 370 (2016).
34. K. Ravikumar, K. S. Krishnan, S. Ramalingam and K. Balu, *Dyes Pigm.*, **72**, 66 (2007).
35. K. Ravikumar, S. Ramalingam, S. Krishnan and K. Balu, *Dyes Pigments*, **70**, 18 (2006).
36. J. N. Sahu, J. Acharya and B. C. Meikap, *J. Hazard. Mater.*, **172**, 818 (2009).
37. G. E. P. Box and N. R. Draper, *Empirical Model-Building and Response Surfaces*, Wiley, Minnesota (1987).
38. N. Draper and J. A. John, *Technometrics*, **30**, 423 (1988).
39. K. Murugesan, A. Dhamija, I. Nam, Y. Kim and Y. Chang, *Dyes Pigments*, **75**, 176 (2007).
40. E. Ch. Khoo, S. T. Ong, Y. T. Hung and S. T. Ha, *Desalin. Water Treat.*, **51**, 7109 (2013).
41. A. Olad, F. Farshi Azhar, M. Shargh and S. Jharfi, *Polym. Eng. Sci.*, **54**, 1595 (2014).
42. F. Bandari, F. Safa and Sh. Shariati, *Arab. J. Sci. Eng.*, **40**, 3363 (2015).
43. S. Sadaf and H. N. Bhatti, *Desalin. Water Treat.*, **57**, 11773 (2016).
44. R. D. Lillie and H. J. Conn, *Conn's biological stains: A handbook on the nature and uses of the dyes employed in the biological laboratory*, Baltimore, Williams & Wilkins (1977).
45. P. Li, Y. J. Su, Y. Wang, B. Liu and L. M. Sun, *J. Hazard. Mater.*, **179**, 43 (2010).
46. K. Petcharoen and A. Sirivat, *Mater. Sci. Eng. B*, **177**, 421 (2012).
47. M. Evans, *Optimization of Manufacturing Processes: A Response Surface Approach*, Carlton House Terrace, London (2003).
48. L. C. A. Oliveira, R. V. R. A. Rios, J. D. Fabris, K. Sapag, V. K. Garg and R. M. Lago, *Appl. Clay Sci.*, **22**, 169 (2003).
49. M. A. Legodi and D. DeWaal, *Dyes Pigments*, **74**, 161 (2007).
50. S. Goyanes, G. R. Rubiolo, A. Salazar, A. Jimeno, M. A. Corcuera and I. Mondragon, *Diamond Relat. Mater.*, **16**, 412 (2007).
51. R. D. Waldron, *Phys. Rev.*, **99**, 1727 (1955).
52. M. Ma, Y. Zhang, W. Yu, H. Y. Shen, H. Q. Zhang and N. Gu, *Colloids and Surfaces A: Physicochem. Eng. Aspects*, **212**, 219 (2003).
53. Z. M. Gao, T. H. Wu and S. Y. Peng, *Acta Phys. Chim. Sin.*, **11**, 395 (1995).
54. K. Yetilmezsoy, S. Demirel and R. J. Vanderbei, *J. Hazard. Mater.*, **171**, 551 (2009).
55. G. Alberghina, R. Bianchini, M. Fichera and S. Fisichella, *Dyes Pigments*, **46**, 129 (2000).
56. G. Derringer and R. Suich, *J. Qual. Technol.*, **12**, 214 (1980).
57. *Design expert statistical software*, Stat-Ease, Inc., 2021 E. Hennepin Avenue, Suite 480, Minneapolis, MN 55413-2726, U.S.A. (2005).
58. S. Lagergren and K. Sven, *Vetenskakad. Handl.*, **24**, 1 (1898).
59. Y. S. Ho and G. McKay, *Process Biochem.*, **34**, 451 (1999).

60. W. J. Weber and J. C. Morris, *J. Sanit. Engg. Div. ASCE*, **89**, 31 (1963).
61. K. Kannan and M. M. Sundaram, *Dyes Pigments*, **51**, 25 (2001).
62. S. J. Allen, G. Mckay and K. Y. H. Khader, *Environ. Pollut.*, **56**, 39 (1989).
63. V. J. P. Poots, G. McKay and J. J. Healy, *J. Water Pollut. Control Fed.*, **50**, 926 (1978).
64. B. H. Hameed, *J. Hazard. Mater.*, **166**, 233 (2009).
65. H. Z. Freundlich, *J. Phys. Chem.*, **57A**, 385 (1906).
66. M. I. Tempkin and V. Pyzhev, *Acta Physiochim.*, USSR **12**, 327 (1940).
67. K. Y. Foo and B. H. Hameed, *Chem. Eng. J.*, **156**, 2 (2010).
68. S. M. Musyoka, H. Mittal, S. B. Mishra and J. C. Ngila, *Int. J. Biol. Macromol.*, **65**, 389 (2014).
69. S. Ghorai, A. Sarkar, M. Raoufi, A. B. Panda, H. Schönherr and S. Pal, *ACS Appl. Mater. Interfaces*, **6**, 4766 (2014).
70. H. Mittal, V. Kumar, Saruchi and S. S. Ray, *Int. J. Biol. Macromol.*, **89**, 1 (2016).